33rd Annual International Conference of the IEEE EMBS
Boston, Massachusetts USA, August 30 - September 3, 2011

A Simulation Framework for Estimating Wall Stress Distribution of Abdominal Aortic Aneurysm

Jing Qin, Jing Zhang, Chee-Kong Chui, Wei-Min Huang,
Tao Yang, Wai-Man Pang, Venkatesh Sudhakar, and Stephen Chang

Abstract— **Abdominal aortic aneurysm (AAA) rupture is believed to occur when the mechanical stress acting on the wall exceeds the strength of the wall tissue. In endovascular aneurysm repair, a stent-graft in a catheter is released at the aneurysm site to form a new blood vessel and protect the weakened AAA wall from the pulsatile pressure and, hence, possible rupture. In this paper, we propose a framework to estimate the wall stress distribution of non-stented/stented AAA based on fluid-structure interaction, which is utilized in a surgical simulation system (IRAS). The 3D geometric model of AAA is reconstructed from computed tomography angiographic (CTA) images. Based on our experiments, a combined logarithm and polynomial strain energy equation is applied to model the elastic properties of arterial wall. The blood flow is modeled as laminar, incompressible, and non-Newtonian flow by applying Navier-Stokes equation. The obtained pressure of blood flow is applied as load on the AAA meshes with and without stent-graft and the wall stress distribution is calculated by fluid-structure interaction (FSI) solver equipped in ANSYS. Experiments demonstrate that our analytical results are consistent with clinical observations.**

I. Introduction

Abdominal aortic aneurysm (AAA) refers to local irreversible ballooning that occurs in human abdominal aorta. If not surgically treated in time, an AAA may rupture, leading to a mortality rate of up to 80%. It was reported that about 15000 deaths from AAA rupture annually in the US alone [1].

There are two AAA repair options: open surgery and endovascular aneurysm repair (EVAR). Open surgery usually carries certain risks and the risks increase with age and the presence of other health condition [2]. EVAR is a preferable option in most cases, where a stent-graft, call an endovascular graft (EVG), in a catheter is passed from the patient's leg artery to the aneurysm site and then released. Once secured in place, the EVG forms a new blood vessel, protecting the weakened AAA wall from the pulsatile blood pressure and, hence, possible rupture [3]. EVAR is preferred over surgery due to its advantages of minimal invasion, early recovery, reduced mortality and morbidity, although long-term follow-up is needed to determine whether these advantages are sustained [4].

In clinical practice, it is difficult to evaluate the rupture risk of an AAA. The traditional criteria for risk evaluation include diameter of AAA, age of patient, ejection fraction, forced expiratory volume, renal insufficiency, and multiple previous abdominal operations [3]. However, all of them are merely based on previous experience and, hence, cannot provide sufficient and exact information on the risk of rupture. For example, in practice, a stent graft is considered needing to be deployed when the maximum diameter of aneurysm exceeds $5cm$ or $5.5cm$ [5]. In reality, some aneurysms rupture when their diameters are less than $5cm$ [6].

AAA rupture is in principle believed to occur when the mechanical stress acting on the wall exceeds the strength of the wall tissue. Therefore, knowledge of the stress distribution in an intact AAA wall could be a more biophysically sound basis in assessing its risk of rupture. Furthermore, stress analysis on a simulated stented AAA could also be used to improve the preoperative planning for precise deployment in EVAR.

Some efforts have been dedicated to investigate the stress distribution on AAA. Baghavan et al propose a systematic framework to noninvasively estimate the wall stress by using 3D reconstructed models [7]. However, biomechanical properties are not configured in their models. Fillinger et al propose a set of methods to computationally determine the stress distribution on the AAA with finite element analysis [8]. But these methods do not take the viscoelastic properties of artery wall into consideration. Recently, a novel microelsctromechanical system (MEMS) sensor is developed to assess spatial- and temporal-varying components of intravascular shear stress (ISS) [9]. However, the accuracy of the assessment need to be further improved before it can be used in prediction of the rupture of AAA.

Recent years have witnessed significant progress in fluid-structure interaction (FSI) simulation. It is suitable to simulate and analyze the interaction of some moveable and deformable structure with an internal or surrounding fluid flow. In this regard, stress analysis of AAA can be considered as a typical FSI problem. Two main approaches exist for FSI simulation problem: monolithic approach [10] and partitioned approach [11].

We propose a novel method to estimate and simulate the wall stress of AAA. The 3D geometric model of AAA is reconstructed based on the segmented results from CTA data. We employ partitioned approach for FSI simulation, where

This work was supported by two projects of A*STAR Singapore.

J. Qin and V. Sudhakar are with the Department of Diagnostic Radiology, National University of Singapore.

J. Qin, C. K. Chui and T. Yang are with the Department of Mechanical Engineering, National University of Singapore.

J. Zhang, T. Yang and W. M. Huang are with the Institute for Infocomm Research, Agency for Science, Technology and Research, Singapore.

W. M. Pang is with the Spatial Media Group, Computer Arts Lab, University of Aizu, Japan.

S. Chang is with the Department of Surgery, National University Hospital, Singapore.

the equations governing the flow and the displacement of structure are solved separately. On one hand, to achieve the actual biomechanical properties of the artery wall, we design a set of *in vitro* experiments on pieces of human abdominal arteries. Based on our experiments, a combined logarithm and polynomial strain energy equation is applied to model the elastic properties of arterial wall. On the other hand, we model the intraaneurysmal blood flow as an incompressible laminar flow. The stress distribution of the flow is applied as load on the inner surface of the artery wall. The final stress distribution on the wall is calculated by the FSI solver of ANSYS. In addition, we also simulated the stend-grafts based on their geometry and biomechanics. Thus, our solution can obtain the stress distribution of both non-stented and stented AAA. Hence, it can be used as both a new criterion in evaluating the rupture risk of AAA and a novel method for preoperative planning of EVAR in a surgical simulation system IRAS, which refers to the Image-guided Robot Assisted Surgical training [12].

II. Method

The pipeline of our method are as follows. The geometric models of aneurysm lumen domain and stent-graft are reconstructed from images of CTA, micro CT and laser scanner. These 3D models are smoothed and refined using *Solidworks*. After meshed and integrated with mechanical properties, the geometric models are converted into biomechanical models that are suitable for finite element analysis. Then we input the blood flow model into ANSYS CFX to calculate the pressure distribution. Finally, the aneurysm models, stent-graft models as well as the pressure distribution are fed into the FSI solver of ANSYS to calculate the stress distribution of AAA.

A. Geometric Modeling

The 3D CTA data (with 1*mm* slice thickness) associated with the aneurysm is first imported into the image data processor for segmentation. Then, Marching cubes algorithm is employed to extract the surface of the segmented luminal structure. The luminal surface is then fed into a FE mesh generator [13] for FE mesh generation.The stent-grafts are modeled from clinical available ones. First, it is scanned using a Micro CT to acquire images. Since the stent-grafts comprise metal wires and fibre cylinder wall, images obtained from the Micro CT have metal dilution noises and invisible fibre. By filtering the noise, metal wires are extracted. Sometimes the fibre can not be identified from the images. A laser scan of the stent-graft is then carried out using the Cyberware rapid 3D digitizer model $3030R - HIREZ$. This machine scans the surface of the stent-graft and obtains its surface points. A high resolution finite element model of stent-graft is constructed based on the geometry information. The material properties of stent-graft are configured based on related literatures [14].

B. Viscoelastic Modeling of Arterial Wall

The mechanical properties of the artery wall are derived from a series of experiments. Stepper motor ($CTP21$ *DANAHER*) driven translational stages are employed to carry out basic motion such as elongation and compression. One large distance laser sensor ($optoNCDT\ 1401-200$, $Micro-epsilon$) is equipped on the translation stage to form a close loop control for positioning. Load cells ($LCM\ UF\ series$) are employed to measure force imposed on specimen. Circulator (*Polyscience* 8106) is employed to circulate the testing medium (Krebs Ringer solution) in the testing environment, and to maintain it at 37^0C.

Based on the experimental data, we use a combined logarithmic and polynomial strain energy function [15] to mathematically model the nonlinear stress function $T^e(\lambda)$:

$$W = \frac{-C_1}{2}\ln(1-u) + \frac{q}{2} \tag{1}$$

With this strain energy equation, $T^e(\lambda)$ can be expressed as follow:

$$\begin{aligned} T^e(\lambda) = (&\frac{2C_1(C_2(\lambda^2 + \frac{2}{\lambda} - 3) + C_4(\lambda^2 - 1))}{1 - \frac{G}{2}} + \\ &2C_5(\lambda^2 + \frac{2}{\lambda} - 3) + 2C_7(\lambda^2 - 1))(\lambda - \frac{1}{\lambda^2}) + \\ &(\frac{2C_1(C_3(\lambda^2 - 1) + C_4(\lambda^2 + \frac{2}{\lambda} - 3))}{1 - \frac{G}{2}} + \\ &2C_6(\lambda^2 - 1) + 2C_7(\lambda^2 + \frac{2}{\lambda} - 3))\lambda \end{aligned} \tag{2}$$

where C_1 to C_7 are material constants.

C. Simulation of Blood Flow

We assume that the temperature of our blood model is nearly constant and there is no heat input into the system and no heat source in the region. Thus we can focus on how to solve the Navier-Stokes which formulates conservation of mass:

$$\frac{D\rho}{Dt} + \rho\nabla\cdot\vec{V} = 0 \tag{3}$$

and momentum:

$$\rho\frac{\partial\vec{V}}{\partial t} = -\rho\vec{V}\cdot\nabla\vec{V} - \nabla p + \mu\nabla^2\vec{V} + \rho\vec{g} \tag{4}$$

where ρ is the density, $\vec{V}$ is the vector velocity field, the vector operator ∇ is defined as $\nabla \equiv \vec{i}\frac{\partial}{\partial x} + \vec{j}\frac{\partial}{\partial y} + \vec{k}\frac{\partial}{\partial z}$, p is the pressure, $\vec{g}$ means the body forces such as gravitational forces, μ is viscosity coefficient.

We consider blood as an incompressible laminar fluid. In general, the constitutive equation of an isotropic incompressible Newtonian fluid is:

$$\gamma_{ij} = -p\phi_{ij} + 2\mu T_{ij} \tag{5}$$

where

$$T_{ij} = \frac{1}{2}(\frac{\partial v_i}{\partial x_j} + \frac{\partial v_j}{\partial x_i}), \tag{6}$$

$$T_{ii} = 0. \tag{7}$$

Here γ_{ij} is the stress tensor, p is the hydrostatic pressure, ϕ_{ij} is the isotropic tensor or Kronecker delta, T_{ij} is the strain-stress tensor, v_i and v_j are the velocity components, and μ is a constant called the coefficient of viscosity.

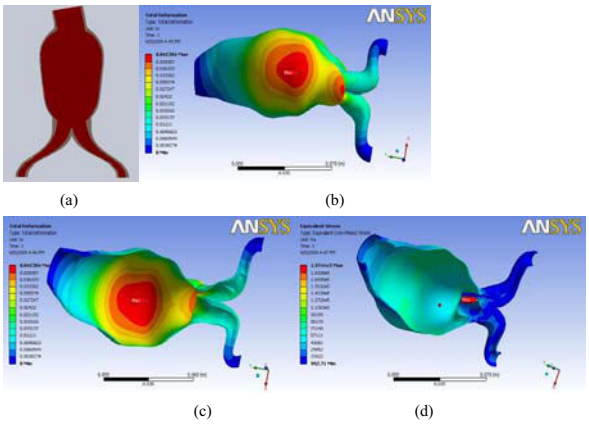

Fig. 1. The simulation results of AAA_1 without stent: (a) cross-section of the geometric model, (b) deformation of aneurysm, (c)maximum deformation is located at the middle of the aneurysm wall, and (d) Maximum von-Misses stress is located at bifurcating part of aneurysm.

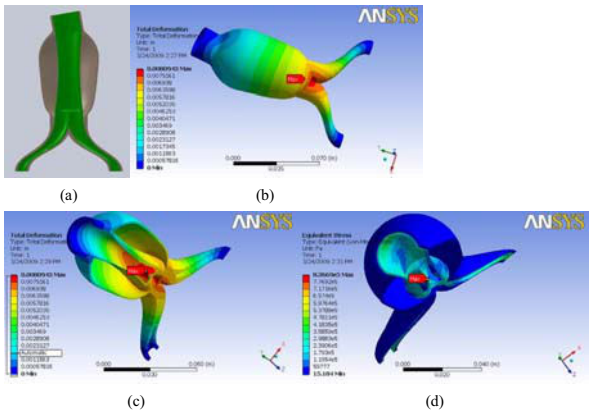

Fig. 2. The simulation results of AAA_1 with stent: (a) cross-section of geometric models, (b) deformation of aneurysm, (c) maximum deformation is located at bifurcating part of stent-graft, and (d) Maximum von-Misses stress is also located at bifurcating part of stent-graft.

We employ ANSYS CFX laminar solver to calculate the pressure distribution of the blood flow based on above equations as well as biomechanical properties of blood. The pressure distribution is then fed into the FSI solver in ANSYS. The interaction between the two analysis typically takes place at the boundary of the simulation models. In our simulation, the fluid-structure interface is at the aneurysm wall and the pressure distribution of blood flow is consider as the load performed on the wall.

III. Results

A. Simulation results

Two sets of geometric models with different shapes of AAA and stent-graft are employed to demonstrate our method. The main parameters of AAA_1 are: the maximum inner aneurysm wall diameter is $48mm$; the proximal neck length is $18mm$; the proximal neck angel is 10^0; and the misalignment of aneurysm body from inlet is $7.93mm$, while the main parameters of AAA_2 are as follows: the maximum inner aneurysm wall diameter is $57mm$; the proximal neck

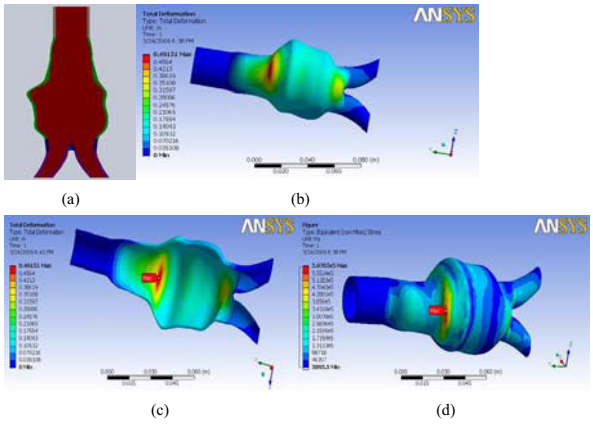

Fig. 3. The simulation results of AAA_2 without stent: (a) cross-section of geometric model, (b) deformation of aneurysm, (c) maximum deformation is located at the middle of the aneurysm wall, and (d) maximum von-Misses stress is also located at the middle of the aneurysm wall.

length is $25mm$; the distal neck length is $10.61mm$; and the misalignment of aneurysm body from inlet is $7.93mm$. Besides the stress distribution, the deformation of aneurysm wall under blood pressure and the maximum von Mises stress are calculated, as they are two important factors indicating rupture risk.

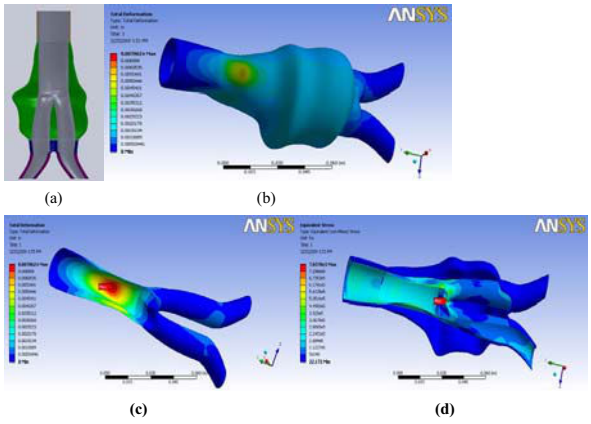

Fig. 4. The simulation results of AAA_2 with stent: (a) cross-section geometric models, (b) deformation of aneurysm, (c) maximum deformation is located at bifurcating part of stent-graft, and (d) maximum von-Misses stress is located at bifurcating part of stent-graft.

Fig. 1 shows the simulation results of non-stented AAA_1. It is observed that aneurysm wall exhibits relatively large deformation ($0.0424m$) and the maximum von Mises ($1.9741 \times 10^5 Pa$) stress is located at the bifurcating part of aneurysm, indicating the easiest place to rupture. Fig. 2 is the simulation results of stented AAA_1. The stent-graft is specially designed for the aneurysm. In this case, the maximum deformation of aneurysm ($0.0081mm$) is located at the bifurcating part of stent-graft. Compared with the results without stent-graft, it is too small to change the shape of the stent-graft. Meanwhile, the maximum von Mises stress ($8.3669 \times 10^5 Pa$) is also located at the bifurcating part of stent-graft. It demonstrates that the stent-graft can protect the aneurysm wall from

rupture well.

Fig. 3 shows the simulation results of Non-stented AAA_2, which has a more complicated shape than AAA_1. The maximum deformation ($0.04915m$) is located at the middle of the aneurysm wall. The location of maximum von Mises stress ($5.9765 \times 10^5 Pa$) is at almost the same same place as the location of maximum deformation. Fig. 4 shows simulation results of stented AAA_2. The maximum deformation ($0.0071m$) is located at the middle of the stent-graft while the maximum von-Mises stress ($7.8578 \times 10^5 Pa$) is located at the bifurcating part of stent-graft. Similarly, the designed stent-graft can protect the aneurysm well. We also invite radiologists to give their preliminary diagnosis based on the information of the two aneurysms. Our simulation results are consistent with their diagnosis.

IV. Discussion and Conclusion

We propose a novel method to estimate the wall stress distribution of non-stented/stented AAA based on fluid-structure interaction simulation. The simulation results suggest that the shape of aneurysm and pressure of blood flow are important factors affecting the location of maximum deformation and distribution of von Mises stress on aneurysm wall. The Young's modulus of the aneurysm wall maintains a negative slope linear relationship with maximum deformation on the aneurysm wall when subjected to same blood pressure. The implantation of stent-graft is very effective in reducing the von Misses stress on the aneurysm wall when the stent-graft is well designed.

In conclusion, FE-based FSI analysis of wall stress distribution for endovascular aneurysm repair(EVAR) is developed. This achievement will contribute to the long term goal of developing a new diagnosis criterion for patient-specific model of EVAR. It could reduce the risks of patient undergoing EVAR, by knowing the regions where the aneurysm is likely to rupture. In addition, this technique can assist doctors in designing an efficient patient-specific stent-graft. Based on the proposed method, we can simulate a stenting procedure using various stent-grafts and provide the possible stress changes and deformation of the vessel wall. In IRAS application, the blood vessels and bile ducts are modeled using the same method and validated using the proposed framework, which enhances the realism of the vessel deformation.

V. ACKNOWLEDGMENTS

This work was funded by two projects: Segmentation, structural modelling and simulation of the aorta and liver for clinical decision-making and treatment planning and Image-guided Robert Assisted Surgical training (IRAS). The first project was funded by The Singapore Bioimaging Consortium (SBIC), the Agency for Science, Technology and Research (A*STAR), Singapore under project number SBIC RP C-008/2006. IRAS was funded by A*STAR, Singapore under grant number 092-148-0072.

References

[1] Z. Li and C. Kleinstreuer, "Effects of major endoleaks on a stented abdominal aortic aneurysm," *J. Biomech. Eng.*, vol. 128, no. 1, pp. 59–68, 2006.

[2] C. B. Ernst, "Abdominal aortic aneurysm," *The New England Journal of Medicine*, vol. 328, no. 16, pp. 1167–1172, 1993.

[3] J. C. Parodi, "Endovascular repair of abdominal aortic aneurysms and other arterial lesions," *J. Vasc. Surg.*, vol. 21, no. 4, pp. 549–557, 1995.

[4] M. Prinssen, E. L. Verhoeven, J. Buth, P. W. Cuypers, M. R. H. M. van Sambeek, R. Balm, E. Buskens, D. E. Grobbee, and J. D. Blankensteijn, "A randomized trial comparing conventional and endovascular repair of abdominal aortic aneurysms," *The New England Journal of Medicine*, vol. 351, no. 16, pp. 1607–1618, 2004.

[5] K. P. Conway, J. Byrne, M. Townsend, and I. F. Lane, "Prognosis of patients turned down for conventional abdominal aortic aneurysm repair in the endovascular and sonographic era: Szilagyi revisited?" *J. Vasc. Surg.*, vol. 33, no. 4, pp. 752–757, 2001.

[6] S. C. Nicholls, J. B. Gardner, M. H. Meissner, and K. H. Johansen, "Rupture in small abdominal aortic aneurysms," *J. Vasc. Surg.*, vol. 28, no. 5, pp. 884–888, 1998.

[7] M. L. Raghavan, D. A. Vorp, M. P. Federle, M. S. Makaroun, and M. W. Webster, "Wall stress distribution on three-dimensionally reconstructed models of human abdominal aortic aneurysm," *J. Vasc. Surg.*, vol. 31, no. 4, pp. 760–769, 2000.

[8] M. F. Fillinger, S. P. Marra, M. L. Raghavan, and F. E. Kennedy, "Prediction of rupture risk in abdominal aortic aneurysm during observation: Wall stress versus diameter," *J. Vasc. Surg.*, vol. 37, no. 4, pp. 724–732, 2003.

[9] L. Ai, H. Yu, W. Dai, S. L. Hale, R. A. Kloner, and T. K. Hsiai, "Real-time intravascular shear stress in the rabbit abdominal aorta," *IEEE Trans Biomed Eng*, vol. 56, no. 6, pp. 1755–1764, 2009.

[10] M. Heil, "An efficient solver for the fully coupled solution of large-displacement fluidcstructure interaction problems," *Computer Methods in Applied Mechanics and Engineering*, vol. 193, no. 1-2, pp. 1–23, 2004.

[11] H. G. Matthies and J. Steindorf, "Partitioned strong coupling algorithms for fluidcstructure interaction," *Computers & Structures*, vol. 81, no. 8-11, pp. 805–812, 2003.

[12] J. Zhang, W. Huang, J. Zhou, J. Qin, B. Lee, T. Yang, J. Liu, Y. Su, C. Chui, and S. Chang, "Gpu-friendly gallbladder modeling for laparoscopic cholecystectomy simulation," in *Proceedings of Biomedical Engineering and Informatics (BMEI), 2010 3rd International Conference on*, 2010, pp. 1872–1876.

[13] C.-K. Chui, Z. Wang, J. Zhang, J. S.-K. Ong, L. Bian, J. C.-M. Teo, C.-H. Yan, S.-H. Ong, S.-C. Wang, H.-K. Wong, and S.-H. Teoh, "A component-oriented software toolkit for patient-specific finite element model generation," *Adv. Eng. Softw.*, vol. 40, no. 3, pp. 184–192, 2009.

[14] Z. Li and C. Kleinstreuer, "Fluid-structure interaction effects on sac-blood pressure and wall stress in a stented aneurysm," *J. Biomech. Eng.*, vol. 127, no. 4, pp. 662–671, 2005.

[15] C. Chui, E. Kobayashi, X. Chen, T. Hisada, and I. Sakuma, "Combined compression and elongation experiments and non-linear modelling of liver tissue for surgical simulation," *Medical and Biological Engineering and Computing*, vol. 42, no. 6, pp. 787–798, 2004.